This paper has been submitted to IEEE for possible publication.
Copyright may be transferred without notice, after which this version may no longer be accessible.

Secure Multi-Hop Relaying in Large-Scale Space-Air-Ground-Sea Integrated Networks

Hyeonsu Lyu, *Student Member, IEEE*, Hyeonho Noh, *Member, IEEE*, Hyun Jong Yang, *Senior Member, IEEE*, and Kaushik Chowdhury, *Fellow, IEEE*

arXiv:2505.00573v1 [eess.SP] 1 May 2025

***Abstract*—As a key enabler of borderless and ubiquitous connectivity, space–air–ground–sea integrated networks (SAGSINs) are expected to be a cornerstone of 6G wireless communications. However, the multi-tiered and global-scale nature of SAGSINs also amplifies the security vulnerabilities, particularly due to the hidden, passive eavesdroppers distributed throughout the network. In this paper, we introduce a joint optimization framework for multi-hop relaying in SAGSINs that maximizes the minimum user throughput while ensuring a minimum strictly positive secure connection (SPSC) probability. We first derive a closed-form expression for the SPSC probability and incorporate this into a cross-layer optimization framework that jointly optimizes radio resources and relay routes. Specifically, we propose an $\mathcal{O}(1)$ optimal frequency allocation and power splitting strategy—dividing power levels of data transmission and cooperative jamming. We then introduce a Monte-Carlo relay routing algorithm that closely approaches the performance of the numerical upper-bound method. We validate our framework on testbeds built with real-world dataset. All source code and data for reproducing the numerical experiments will be open-sourced.**

***Index Terms*—Secure connection probability, non-terrestrial network, multi-hop relay, Monte-Carlo relay routing, max-min throughput.**

I. Introduction

The era of hyper-connectivity begins. SpaceX's reusable launch vehicles have paved the way for extending commercial satellite communications to a broader user base [1], and initiatives such as Google's Project Loon [2] and Aerostar's Thunderhead [3] have established the technical foundations for high-altitude platforms (HAPs) networks. Moreover, the advances in sea surface [4] and underwater base stations [5], other forms of borderless networks, signals a big paradigm shift: a global-scale integrated network [6], [7]. NTNs break down national boundaries, lay the groundwork for an interplanetary internet, and provide communication infrastructure across all regions of the Earth. Ubiquitous connectivity in line with this trend has emerged as a primary objective for 6G wireless [8], driving active discussions on standards for non-terrestrial networks [9]–[11]. The integration of these vertical, heterogeneous network layers stands to transcend the limitations of terrestrial networks.

To enjoy such merits of the space-air-ground(-sea) integrated networks (SAG(S)INs), various technical challenges have been studied accordingly in both industry and academia [12]–[19]. Consequently, numerous techniques have been proposed to combine the complementary strengths of heterogeneous platforms, thereby achieving ubiquitous global coverage and strengthening link reliability by leveraging the multiple communication channels [6]. However, the wide communication coverage of SAGSIN and the participation of numerous heterogeneous nodes can intrinsically intensify the possibility of eavesdropper intrusion [7], [20]. Safeguarding the integrity and confidentiality of SAGSIN is critical in scenarios where the secrecy requirements are exceptionally high, such as maritime energy transportation and military operations. Moreover, eavesdroppers can achieve considerable SNR with minimal gain as LEO and HAPs emit signals via line-of-sight channels over vast areas, exponentially expanding the attack surface. Therefore, physical-layer security must be employed in SAGSIN to protect information of legitimate users.

Ensuring secrecy for network nodes in SAGSINs presents several technical challenges. Users in the SAGSIN must traverse multiple base station nodes to access the core internet [21]. This indicates that secrecy must be maintained across multiple relay hops, each of which constitutes a potential vulnerability exploitable by adversaries [22]. Numerous studies have explored secure communications in SAGSINs where HAPs serve as intermediate nodes to bridge satellites and ground terminals in two-hop relay systems [12]–[15]. However, ensuring secure communications across multi-hop relays in SAGSINs still needs further investigation.

Delivering high throughput to users while ensuring security presents another significant challenge. In SAGSINs, optimizing radio resources to maximize throughput under security constraints is inherently intractable as acquiring accurate channel state information (CSI) of hidden eavesdroppers (Eves) is practically infeasible [23], [24]. However, many studies focus on optimizing the relay itself for given CSI, while the joint optimization of relay and radio resource management (RRM) in SAGSINs remains an open problem.

These challenges motivate the following research question:

How can high-throughput, secure SAGSIN relay be established without Eve's channel information?

This research question has rarely been addressed within the context of secure SAGSIN research, as shown in Table I. Unlike prior works that only optimize secure relaying in NTNs, we introduce a joint optimization framework for multi-hop relaying that maximizes the minimum user throughput while ensuring a prescribed strictly positive secure connection (SPSC) probability against unknown or passive eavesdroppers.

The contributions of this work are summarized as follows:

- ***Cross-layer secure relaying framework***: We propose

TABLE I
SUMMARY OF THE RELATED WORKS IN SEC. II

Ref.	Archit.	Eve.	RA	PC	Jamming	Relay
[12]	SAGIN	Known	✗	✗	✗	Two-hop
[13]–[15]	SAGIN	Known	✗	✓	✓	Two-hop
[16]	SAGIN	Known	✗	✓	✗	-
[17]	SAGIN	Known	✗	✓	✗	Two-hop
[25], [26]	SAGIN	Unknown	✗	✗	✗	Multi-hop
[27]	UAV net.	Unknown	✗	✗	✗	Multi-hop
[18]	UAV net.	Known	✗	✗	✓	Multi-hop
[19]	SGIN	Known	✗	✗	✓	Multi-hop
[28]	SGIN	Known	✗	✗	✗	Multi-hop
Ours	SAGSIN	Unknown	✓	✓	✓	Multi-hop

* RA: Frequency resource allocation, PC: Power control, S(A)GIN: Space(-air)-ground integrated network.

a cross-layer framework for secure multi-hop relaying in large-scale SAGSINs that optimizes the max-min throughput **without Eve's channel information**, enabling new forms of secure communications that were previously unattainable. This formulation greatly simplifies the optimization process compared to conventional max-min secrecy rate approaches, while achieving comparable performance to the max-min secrecy problem (Fig. 8).

- ***Efficient solution design***: We develop globally optimal closed-form solutions for radio resource management (RRM) with $\mathcal{O}(1)$ computational complexity (**Theorem 1**), achieving the optimal frequency allocation, transmission and jamming power control for a given routing topology. Based on this, we propose a Monte-Carlo relay routing (MCRR) algorithm (Alg. 1) with $\mathcal{O}(N \log N)$ complexity among N nodes. Our method consistently achieves max-min throughput within approximately 5% of the upper bound under various secure SAGSIN simulation settings (Figs. 6–9).
- ***Real-world SAGSIN testbed***: We validate the proposed framework and solver using real-world data of terrestrial, HAPs, LEO base stations, and vessel data. To the best of our knowledge, this is **the first real-world SAGSIN testbed** built upon a real-world dataset including HAPs base stations. The demonstrations on the testbeds not only demonstrate the practicality and superiority of the RRM and routing algorithm (Fig. 10), but also illustrate that the framework can immediately adapt to changes in the security environment (Fig. 11).

II. RELATED WORKS

Recent studies have explored diverse approaches to secure communication in SAGSIN. We survey both general physical-layer security strategies and secure routing approaches in the broader context of NTNs, including satellite networks and HAP networks. The research works can be summarized as shown in Table. I.

A. Secure Communications in SAGSINs

[12] proposes an aerial bridge scheme using UAVs to form secure tunnels and reduce the eavesdropping footprint. [13] enhances secrecy rate via a joint UAV deployment and power allocation using successive convex approximation to decouple complex multi-layer constraints, and [14] further enhances security by optimizing UAV trajectory and power with a hybrid FSO/RF scheme that mitigates RF vulnerabilities through optical satellite links. Similarly, [15] combines UAV-assisted non-orthogonal multiple access with cooperative jamming to counter both internal and external eavesdropping threats in SAGINs. [16] proposes a label-free deep learning framework that dynamically selects access strategies to maximize sum secrecy rate. [17] optimizes HAPs trajectories and beamforming by employing a generative AI-based DRL framework for proactive adaptation and improved secrecy energy efficiency under dynamic channel changes.

These studies have contributed to improving various secrecy utilities in small-scale SAGSINs with less than two-hops under the assumption of perfect knowledge of Eve's channels. However, it is essential to investigate wide-area multi-hop communications under imperfect knowledge of Eve's channel, as SAGSINs are fundamentally intended to enable ubiquitous global connectivity.

B. Secure Routing in NTNs

[25] presents a hybrid SDN architecture with hierarchical control to enable secure and quality-of-service (QoS)-aware routing in SAGINs. [26] design an artificial bee colony-based routing protocol for UAV networks, significantly improving routing performance and consensus efficiency in dynamic environments. Meanwhile, [27] proposes a position-aware routing protocol for airborne mesh networks to efficiently mitigate threats from wormhole and blackhole attacks. Furthermore, [18] propose a secure, energy-efficient UAV relay framework using collaborative beamforming to jointly enhance secrecy and reduce propulsion energy consumption. Additionally, [19] analyzes security–reliability trade-offs in satellite–terrestrial relay networks with imperfect CSI by introducing a friendly jammer, deriving closed-form expressions for outage and intercept probabilities. [28] jointly designs secure relay selection and user scheduling for hybrid satellite–terrestrial relay networks, deriving closed-form expressions for average secrecy capacity.

These studies have enabled secure communication over broader geographic areas through multi-hop relaying. However, these studies may not achieve optimal communication utility as they either assume fixed physical channels for routing, or do not consider the trade-off between transmission and jamming power. Therefore, a cross-layer design to jointly optimize RRM and relay routing is required in multi-hop SAGSINs.

III. SCENARIO DESCRIPTION

A. Scenario Description

This paper aims to construct a secure relaying route in the SAGSIN, with consideration of radio resources, keeping the

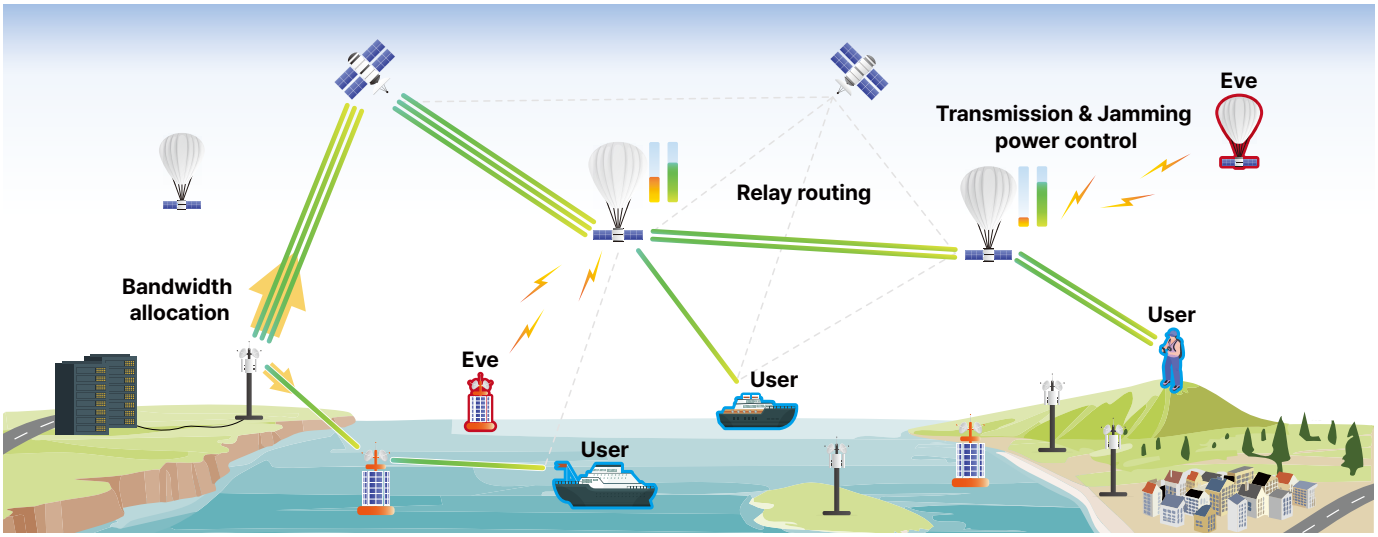

Fig. 1. Illustration of the target scenario in secure multi-hop relaying for SAGSINs. The diagram shows a source node relaying data to multiple users via intermediate nodes. At each relay hop, the nodes transmit both data and predefined jamming signals to degrade the Eves' signal quality, whose locations are modeled as uniformly distributed across the space, air, ground, and sea layer. Each node dynamically allocates bandwidth between data transmission and jamming to maximize the minimum user throughput.

SPSC probability above a certain threshold in the presence of the hidden Eves. Fig. 1 illustrates the target scenario with three control variables. The SAGSIN relay adopts the decode-and-forward scheme [29] and operates in a half-duplex manner, where the throughput is conversely proportional to the number of hops [30]. The nodes transmit predefined jamming signals with data signal to degrade Eve's wiretap ability by reducing the SINR of the wiretap channel [22]. Meanwhile, legitimate nodes recover the original data by cancelling the jamming signals with predefined patterns [31].

The index set of Eves is defined as $\mathcal{M}$. We assume that Eves are present at each network layer to wiretap legitimate communications. The Eves are assumed to be non-colluding as the SAGSIN's extensive geographic dispersion of nodes makes cooperative wiretap channels logistically unfeasible and the limitations in memory and compute of mobile Eves hinder storing raw I/Q signals. We assume that *the location and channel model of Eves are unknown*, where Eves in each network layer are independently distributed following the homogeneous Poisson point processes (HPPP) with density $\lambda_1, \lambda_2, \lambda_3$, and λ_4 for the space, air, ground, and sea network layers, respectively.

We define the index set of nodes as $\mathcal{I} = \{0, 1, ..., I\}$. A total of U users are served through the multi-hop relays, where the user index set is denoted as $\mathcal{U} = \{1, ..., U\}$. The binary variable $x_{(i,j)} \in \{0, 1\}$ indicates whether there exists a hop between the i-th and j-th nodes. The location of the i-th node and Eve e are denoted as $\boldsymbol{p}_i$ and $\boldsymbol{p}_e$, respectively.

B. Propagation Model and Secrecy Metrics

The instantaneous received SNR of the legitimate hop between node i and j, if any, can be given as

$$\mathrm{SNR}^{\mathsf{s}}_{(i,j)} = \frac{\rho_i |h^{\mathsf{s}}_{(i,j)}|^2}{n_0 (d^{\mathsf{s}}_{(i,j)})^{\alpha_i}} \tag{1}$$

where $d^{\mathsf{s}}_{(i,j)} = \|\boldsymbol{p}_i - \boldsymbol{p}_j\|_2$ is a distance between; ρ_i is the power density; and $h_{(i,j)}$ is small-scale Rayleigh fading channel. The path loss exponent α_i is determined based on the network layer in which node i is located. As nodes can decode and cancel the predefined jamming signal, the SINR of legitimate links are not affected by jamming. Meanwhile, the SNR of wiretap link for node i and Eve k can be defined as

$$\mathrm{SNR}^{\mathsf{e}}_{i,e} = \frac{\rho_i |h^{\mathsf{e}}_{i,e}|^2}{(\sigma_i + n_0)(d^{\mathsf{e}}_{i,e})^{\alpha_i}} \tag{2}$$

where σ_i is the power level of the transmitted jamming signal [32]–[34]. For all links, we consider that $|h^{\mathsf{s}}_{(i,j)}|^2$ and $|h^{\mathsf{e}}_{i,e}|^2$ follow exponential distribution $\mathsf{Exp}(1)$. The entire transmission power of node i is limited to P; and the minimum transmission power level is defined as P_i, denoted as

$$\rho_i + \sigma_i \leq P, \ p_i \geq P_i \ \forall i \in \mathcal{I} \tag{3}$$

As the multiple non-colluding Eves can wiretap the legitimate transmission, the secrecy capacity of the link between nodes i and j is defined as

$$C_{(i,j)} = \left[\log_2 \left(1 + \mathrm{SNR}^{\mathsf{s}}_{(i,j)}\right) - \log_2 \left(1 + \max_{e \in \mathcal{M}} \mathrm{SNR}^{\mathsf{e}}_{i,e}\right) \right]^+. \tag{4}$$

Then, as introduced in [35]–[38], the SPSC probability between node i and j is defined as

$$\mathbb{P}_{(i,j)} = \mathbb{P}(C_{(i,j)} > 0). \tag{5}$$

The closed-form derivation of (5) **will be presented in** (22)**.**

C. Multi-hop Relay Model: Graph-Theoretic Viewpoint

a) Graph topology: The routing problem is generally considered as finding a sub-graph of directed graph $\mathcal{G}_{\mathrm{all}} = (\mathcal{N}, \mathcal{E})$ where $\mathcal{N} \subset \mathcal{I} \cup \mathcal{U}$ and $\mathcal{E} \subset \{(i,j) | i, j \in \mathcal{N}\}$. This

represents that nodes and users are the graph nodes and the relay hops are the graph edges [39], [40].

We assume a spanning tree (ST) topology, which refers to an acyclic graph where all nodes have a single path to the root node [41]. This assumption can be relaxed into a directed acyclic graph (DAG) topology, another topology discussed in the 3GPP standards [42], where nodes can be backhauled by multiple parent nodes. However, the DAG topology requires a sophisticated channel and data management system to synchronize and integrate multiple backhaul links, which is not suitable for non-terrestrial network where node distances can vary significantly.[1]

For graph $\mathcal{G}$ to have ST topology, $\mathcal{G}$ must satisfy several constraints.

$$x_{(i,j)} = \begin{cases} 1, \text{ if } (i,j) \in \mathcal{E} \\ 0, \text{ otherwise} \end{cases} \tag{6}$$

to indicate whether edge (i,j) belongs to the graph $\mathcal{G}$ and edge (i,j) belongs to the relay path of user u. There must be no edges entering to the root node 0, denoted as

$$\sum_{i \in N} x_{(i,0)} = 0. \tag{7}$$

In contrast, every other node should have exactly one entering edge, which is

$$\sum_{j \in \mathcal{N}} x_{(j,i)} = 1, \forall i \in \mathcal{N} \setminus \{0\} \tag{8}$$

We introduce the following *cut-based* constraint, which is a standard expression to guarantee graph $\mathcal{G}$ has ST topology. For any non-empty subset $S \subset \mathcal{N} \setminus \{0\}$, there must be at least one selected edge (i,j) with $i \in \mathcal{N} \setminus S$ and $j \in S$, which denoted as

$$\sum_{i \notin S,\, j \in S} x_{(i,j)} \geq 1, \quad \forall\, S \subset \mathcal{N} \setminus \{0\},\ S \neq \emptyset. \tag{9}$$

This constraint prevents any group of nodes from being disconnected or forming a closed loop that excludes the root. In other words, *all nodes remain connected to the root node*. Consequently, each node is guaranteed a directed path originating from the root, satisfying the ST topology. Then, we define a relay path from node 0 to user u as $\mathcal{E}_u$ and binary variable $x_{(i,j),u}$ as

$$x_{(i,j),u} = \begin{cases} 1, \text{ if } (i,j) \in \mathcal{E}_u \\ 0, \text{ otherwise} \end{cases} \tag{10}$$

to indicate whether edge (i,j) belongs to the relay path of user u.[2]

[1]Nonetheless, the system model can also be applied to the relay with directed acyclic graph topology by changing the graph topology constraints.

[2]The system model considers cross-layer optimization of both network-layer routing and physical-layer resource, so both $x_{(i,j)}$ and $x_{(i,j),u}$ are required to consider the routing and radio resource optimization, respectively.

b) Relay throughput: The nodes dynamically allocate bandwidth and transmit power on the backhaul link to maximize the network utility. We define $\beta_{(i,j),u}$ to represent the allocated bandwidth of user u at link (i,j); and the spectral efficiency $\gamma_{(i,j)}$ between node i and j as[3]

$$\gamma_{(i,j)} = \log_2\left(1 + \mathrm{SNR}^{\mathsf{s}}_{(i,j)}\right). \tag{11}$$

The relay throughput of user u is defined as the minimum link capacity divided by the number of hops, denoted as

$$\eta_u = \min_{(i,j) \in \mathcal{E}_u} \frac{\beta_{(i,j),u}\gamma_{(i,j)}}{h_u}, \tag{12}$$

where $\mathcal{E}_u = \{(i,j) : x_{(i,j),u} = 1\}$ is the relay path of user u and $h_u = \sum_{(i,j) \in \mathcal{E}} x_{(i,j),u}$ is the number of hops for user u. Then, the minimum throughput of the system is defined as

$$\min_{u \in \mathcal{U}} \eta_u = \min_{\substack{u \in \mathcal{U} \\ (i,j) \in \mathcal{E}_u}} \frac{\beta_{(i,j),u}\gamma_{(i,j)}}{h_u}. \tag{13}$$

IV. Problem Formulation and Proposed Solution

We aim to maximize the minimum throughput across the entire system, ensuring fair service for users accessing the core internet via multiple hops. Guaranteeing a SPSC probability in multi-hop relay networks while maximizing throughput has been first pioneered by [43]–[45]. Similarly, the relay routing problem that ensures users' QoS while achieving the optimal secure connection probability has also been investigated [46], [47]. However, there has been no attempt to optimize the max-min throughput of the multi-hop relaying system, guaranteeing the SPSC probability.

Let $\mathbf{B} = \{\beta_{(i,j),u} : i,j \in \mathcal{N}, u \in \mathcal{U}\}$, $\mathbf{P} = \{\rho_i : i \in \mathcal{N}\}$, and $\mathbf{J} = \{\sigma_i : i \in \mathcal{N}\}$. The max-min throughput problem is formulated as:

$$\boldsymbol{\mathcal{P}1}: \max_{\mathcal{G},\mathbf{B},\mathbf{P},\mathbf{J}} \min_{\substack{u \in \mathcal{U}, \\ (i,j) \in \mathcal{E}_u}} \frac{\beta_{(i,j),u}\gamma_{(i,j)}}{h_u} \tag{14a}$$

$$\text{s.t. } x_{(i,j)}\mathbb{P}_{(i,j)} \geq \tau, \tag{14b}$$

$$(7),\ (8),\ (9) \tag{14c}$$

$$\sum_{j \in \mathcal{N}} \sum_{u \in \mathcal{U}} \beta_{(i,j),u} \leq B, \tag{14d}$$

$$\rho_i + \sigma_i \leq P, \tag{14e}$$

$$\beta_{(i,j),u} \geq 0, \rho_i \geq P_i, \sigma_i \geq 0. \tag{14f}$$

Constraint (14b) represents the threshold of the secrecy connection probability; (14c) is related to the graph topology; (14d) is the frequency resource constraint; (14e) pertains to the transmission and jamming power constraint; and (14f) ensures the positivity of resource variables.

There are two main challenges to solve Problem $\boldsymbol{\mathcal{P}1}$. The formulated problem is a mixed-integer non-convex problem due to the ST topology assumption and max-min throughput objective. Specifically, the tight coupling between graph and radio resource variables in the objective makes it challenging to search the optimal solution. Finding the exact form of

[3]The ergodic spectral efficiency $\mathbb{E}_{|h^{\mathsf{s}}_{(i,j)}|^2}\left[\log_2(1 + \mathrm{SNR}^{\mathsf{s}}_{(i,j)})\right]$ is approximated as $\log_2\left(1 + \rho_i / [n_0 (d^{\mathsf{s}}_{(i,j)})^{\alpha_i}]\right)$ by using the Jensen's inequality.

(14b) is another challenge. The SPSC probability can alternatively be computed using numerical methods; however, this approach may result in significant computational overhead and restrict the application of analytic methods for identifying acceptable solutions within a limited computational budget. This paper tackles the challenges above by grafting the graph-optimization to radio resource allocation; and by deriving the exact form of the SPSC probability.

A. Closed-form Derivation of a Single-Hop SPSC Probability

For a hop between node i and j, the SPSC probability is defined from (4) as

$$\mathbb{P}_{(i,j)} = \mathbb{P}\left(\log_2\left(\frac{1+\mathrm{SNR}^{\mathsf{s}}_{(i,j)}}{1+\max_{e\in\mathcal{M}}\mathrm{SNR}^{\mathsf{e}}_{i,e}}\right)>0\right) \tag{15}$$

$$= \mathbb{P}\big(\mathrm{SNR}^{\mathsf{s}}_{(i,j)} > \max_{e\in\mathcal{M}}\mathrm{SNR}^{\mathsf{e}}_{i,e}\big) \tag{16}$$

$$= \mathbb{E}_{h^{\mathsf{s}}_i,\mathcal{M}}\Big[\prod_{e\in\mathcal{M}}\mathbb{P}\big(\mathrm{SNR}^{\mathsf{s}}_{(i,j)} > \mathrm{SNR}^{\mathsf{e}}_{i,e}\big)\Big]. \tag{17}$$

Equation (17) is derived from the characteristic of HPPP and the property of maximum operation in the probability, which is $\mathbb{P}(\max\{\gamma_1,...,\gamma_n\}>C) = \mathcal{P}(\gamma_1>C,...,\gamma_n>C)$ for any r.v. $\gamma_1,...,\gamma_n$ and $C\in\mathbb{R}$.

We define $\lambda_i \in \{\lambda_1,\lambda_2,\lambda_3,\lambda_4\}$ as the Eve density of the network layer that node i belongs to. The probability generating functional of HPPP results in $\mathbb{E}_{\mathcal{M}}[\prod_{e\in\mathcal{M}} f(\boldsymbol{p}_e)] = \exp\big(-\lambda_i\int_{\mathbb{R}^2} 1-f(\boldsymbol{p}_e)d\boldsymbol{p}_e\big)$. Then, $\mathbb{P}_{(i,j)}$ can be given by

$$\mathbb{P}_{(i,j)} = \mathbb{E}_{h^{\mathsf{s}}_i}\left[\exp\Big[-\lambda_i\int_{\mathbb{R}^2}\mathbb{P}\big(\mathrm{SNR}^{\mathsf{s}}_{(i,j)} < \mathrm{SNR}^{\mathsf{e}}_{i,e}\big)\,d\boldsymbol{p}_e\Big]\right] \tag{18}$$

$$= \mathbb{E}_{h^{\mathsf{s}}_i}\left[\exp\Big[-\lambda_i\int_{\mathbb{R}^2}\mathbb{P}\Big(\mathrm{SNR}^{\mathsf{s}}_{(i,j)} < \frac{\rho_i|h^{\mathsf{e}}_{i,e}|^2}{(\sigma_i+n_0)(d^{\mathsf{e}}_{i,e})^{\alpha_i}}\Big)d\boldsymbol{p}_e\Big]\right].$$

Then, since $|h^{\mathsf{e}}_{i,e}|$ is also exponentially distributed, (18) can be further evaluated as

$$\mathbb{P}_{(i,j)} = \mathbb{E}_{h^{\mathsf{s}}_i}\left[\exp\Big[-\lambda_i\times \int_{\mathbb{R}^2}\exp\Big(-\frac{(\sigma_i+n_0)(d^{\mathsf{e}}_{i,e})^{\alpha_i}}{\rho_i}\mathrm{SNR}^{\mathsf{s}}_{(i,j)}\Big)\,d\boldsymbol{p}_e\Big]\right]. \tag{19}$$

We can obtain the lower bound approximation of (19) by applying Jensen's inequality, which is

$$\mathbb{P}_{(i,j)} = \exp\Bigg[-\lambda_i\times \int_{\mathbb{R}^2}\underbrace{\mathbb{E}_{h^{\mathsf{s}}_i}\Big[\exp\Big(-\frac{(\sigma_i+n_0)(d^{\mathsf{e}}_{i,e})^{\alpha_i}}{\rho_i}\mathrm{SNR}^{\mathsf{s}}_{(i,j)}\Big)\Big]}_{\text{(a)}}\,d\boldsymbol{p}_e\Bigg]. \tag{20}$$

As random variable $X = \mathrm{SNR}^{\mathsf{s}}_{(i,j)}$ follows exponential distribution $\mathsf{Exp}\big(n_0(d^{\mathsf{s}}_{(i,j)})^{\alpha_i}/\rho_i\big)$, (a) can be directly computed as

$$(a) = \int_0^\infty \exp(-\lambda x)f_X(x)dx = \int_0^\infty \tau\exp[-(\lambda+\tau)x]dx$$

$$= \frac{n_0(d^{\mathsf{s}}_{(i,j)})^{\alpha_i}}{(\sigma_i+n_0)(d^{\mathsf{e}}_{i,e})^{\alpha_i}+n_0(d^{\mathsf{s}}_{(i,j)})^{\alpha_i}}, \tag{21}$$

for $\lambda = (\sigma_i+n_0)(d^{\mathsf{e}}_e)^{\alpha_i}/\rho_i$ and $\tau = n_0(d^{\mathsf{s}}_{(i,j)})^{\alpha_i}/\rho_i$. Then, $\mathbb{P}_{(i,j)}$ can be formulated as

$$\mathbb{P}_{(i,j)} = \exp\Bigg[-\lambda_i\int_{\mathbb{R}^2}\frac{n_0(d^{\mathsf{s}}_{(i,j)})^{\alpha_i}}{(\sigma_i+n_0)(d^{\mathsf{e}}_{i,e})^{\alpha_i}+n_0(d^{\mathsf{s}}_{(i,j)})^{\alpha_i}}\,d\boldsymbol{p}_e\Bigg]$$

$$= \exp\Bigg[-\kappa_i\Big(\frac{n_0}{\sigma_i+n_0}\Big)^{\frac{2}{\alpha_i}}(d^{\mathsf{s}}_{(i,j)})^2\Bigg] \tag{22}$$

where $\kappa_i = \pi\lambda_i\sin^{-1}(\frac{2}{\alpha_i}\pi)$. The Eve density λ_i and the propagation exponent α_i are determined by the network layer to which node i belongs. Equation (22) can be derived by the below lemma:

Lemma 1. $\int_{\mathbb{R}^2}\frac{c}{\|\boldsymbol{x}\|_2^\alpha+c}d\boldsymbol{x} = \pi\sin^{-1}\left(\frac{2}{\alpha}\pi\right)\cdot c^{2/a}$ *for* $c>0$.

Proof. A detailed derivation is provided in Appendix A. □

The integral diverges when $\alpha = 2$, which implies that mathematically guaranteed secure connection in the free-space cannot be achieved.

B. Optimal Frequency Resource Allocation

We first look into how the optimal $\mathbf{B}$ is obtained for given $\mathcal{G},\mathbf{P},\mathbf{J}$.

$$\boldsymbol{\mathcal{P}2}: \min_{\mathbf{B},\eta}\ \frac{1}{\eta} \tag{23a}$$

$$\text{s.t. } \beta_{(i,j),u}\gamma_{(i,j)}h_u^{-1} \geq x_{(i,j),u}\eta \tag{23b}$$

$$\sum_{j\in\mathcal{N}}\sum_{u\in\mathcal{U}}\beta_{(i,j),u} \leq B. \tag{23c}$$

The Lagrangian function of $\boldsymbol{\mathcal{P}2}$ is

$$\mathcal{L}(\mathbf{B},\eta,\boldsymbol{\lambda},\mu) = \frac{1}{\eta} + \sum_{\lambda_{(i,j),u}\in\boldsymbol{\lambda}}\lambda_{(i,j),u}\Big(x_{(i,j),u}\eta - \frac{\beta_{(i,j),u}\gamma_{(i,j)}}{h_u}\Big) + \mu\Big(\sum_{j\in\mathcal{N}}\sum_{u\in\mathcal{U}}\beta_{(i,j),u} - B\Big) \tag{24}$$

for $\boldsymbol{\lambda} = \{\lambda_{(i,j),u} : i,j\in\mathcal{N}, u\in\mathcal{U}\}$. The first-order optimality condition on (24), $\delta\mathcal{L}/\delta\eta = 0,\ \delta\mathcal{L}/\delta\beta_{(i,j),u} = 0$, gives

$$\eta = \Big(\sum\lambda_{(i,j),u}x_{(i,j),u}\Big)^{-\frac{1}{2}},\ \lambda_{(i,j),u} = \frac{\mu h_u}{\gamma_{(i,j)}}. \tag{25}$$

The optimal resource allocation $\beta^*_{(i,j),u}$ occurs when all frequency resources are fully utilized, which corrensponds to the equality condition of (23c). Otherwise, we have $\mu = \lambda_{(i,j),u} = 0$ and η in (25) is not defined according to complementary slackness of the KKT conditions. Similarly, the equality condition of (23b) should be satisfied as well.

This can be expressed mathematically as

$$x_{(i,j),u}\eta - \frac{\beta^*_{(i,j),u}\gamma_{(i,j)}}{h_u} = 0,\ \sum_{j\in\mathcal{N}}\sum_{u\in\mathcal{U}}\beta^*_{(i,j),u} = B. \tag{26}$$

Solving the above equations with respect to $\beta^*_{(i,j),u}$ results in

$$\beta^*_{(i,j),u} = B\frac{x_{(i,j),u}h_u}{\gamma_{(i,j)}}\Big(\sum_{j\in\mathcal{N}}\sum_{u\in\mathcal{U}}\frac{x_{(i,j),u}h_u}{\gamma_{(i,j)}}\Big)^{-1}. \tag{27}$$

C. Optimal Power Allocation

For fixed $\mathcal{E}$, we can reformulate $\mathcal{P}\mathbf{1}$ by plugging in (27) and introducing an auxiliary variable μ as in $\mathcal{P}\mathbf{2}$ as

$$\mathcal{P}\mathbf{3}: \min_{\mathbf{P},\mathbf{J},\eta} \quad \frac{1}{\eta} \tag{28a}$$

$$\text{s.t.} \quad \eta \sum_{j\in\mathcal{N}} \sum_{u\in\mathcal{U}} \frac{x_{(i,j),u} h_u}{\gamma_{(i,j)}} \leq B, \tag{28b}$$

$$\text{(14b)}, \ \text{(14e)}, \ \rho_i \geq P_i, \ \sigma_i \geq 0. \tag{28c}$$

We first simplify the constraints and then mathematically prove that the natural argument: *The optimal throughput is achieved at the maximum transmission power allowed by the system*.

As $d^{\mathsf{s}}_{(i,j)}$ are fixed for given $\mathcal{E}$, the SPSC probability (22) can be viewed as a function of σ_i, denoted as $\mathbb{P}_{(i,j)}(\sigma_i)$. As $\mathbb{P}_{(i,j)}(\sigma)$ is a monotonic increasing function, the constraint (14b) can be redefined as

$$\sigma_i \geq \mathbb{P}^{-1}_{(i,j)}(\tau) = x_{(i,j)} \Big[\Big(\frac{\kappa_i (d^{\mathsf{s}}_{(i,j)})^2}{-\ln \tau} \Big)^{\frac{\alpha_i}{2}} - 1 \Big] n_0. \tag{29}$$

We remark that σ_i is bounded by the maximum of the $\mathbb{P}^{-1}_{(i,j)}(\tau)$, which is determined by the farthest link from node i. Combined with $\sigma_i \geq 0$, the constraint can be given by

$$\sigma_i \geq \tau_i = \Big[\Big(\frac{\kappa_i (d^{\mathsf{max}}_i)^2}{-\ln \tau} \Big)^{\frac{\alpha_i}{2}} - 1 \Big]^+ n_0 \tag{30}$$

where $d^{\mathsf{max}}_i = \max_{j:(i,j)\in\mathcal{E}} x_{(i,j)} d^{\mathsf{s}}_{(i,j)}$.

Then, Problem $\mathcal{P}\mathbf{3}$ can be simplified as

$$\mathcal{P}\mathbf{3}: \max_{\mathbf{P},\eta} \quad \eta \tag{31a}$$

$$\text{s.t.} \quad \eta \sum_{j\in\mathcal{N}} \sum_{u\in\mathcal{U}} \frac{x_{(i,j),u} h_u}{\gamma_{(i,j)}} \leq B, \tag{31b}$$

$$\rho_i + \sigma_i \leq P, \ \rho_i \geq P_i, \ \sigma_i \geq \tau_i. \tag{31c}$$

The Lagrangian function of $\mathcal{P}\mathbf{3}$ is

$$\mathcal{L}(\mathbf{P}, \eta, \boldsymbol{\lambda}, \boldsymbol{\mu}, \boldsymbol{\nu}, \boldsymbol{\xi}) = \eta - \sum_{i\in\mathcal{I}} \lambda_i \Big[B - \eta \sum_{j\in\mathcal{N}} \sum_{u\in\mathcal{U}} \frac{x_{(i,j),u} h_u}{\gamma_{(i,j)}} \Big] + \sum_{i\in\mathcal{I}} \mu_i (P - \rho_i - \sigma_i) + \sum_{i\in\mathcal{I}} \nu_i (\rho_i - P_i) + \sum_{i\in\mathcal{I}} \xi_i (\sigma_i - \tau_i). \tag{32}$$

Then, the derivatives of Lagrangian function are provided as

$$\frac{\delta \mathcal{L}}{\delta \eta} = 1 + \sum_{i\in\mathcal{I}} \lambda_i \sum_{j\in\mathcal{N}} \sum_{u\in\mathcal{U}} \frac{x_{(i,j),u} h_u}{\gamma_{(i,j)}} = 0, \tag{33}$$

$$\frac{\delta \mathcal{L}}{\delta \rho_i} = \lambda_i \eta \frac{\delta A_i}{\delta \rho_i} - \mu_i + \nu_i = 0, \tag{34}$$

$$\frac{\delta \mathcal{L}}{\delta \sigma_i} = -\mu_i + \xi_i = 0. \tag{35}$$

Also, the complementary slackness condition indicates $\nu_i = 0$ and $\sigma_i > 0$ since the nodes in the network can transmit signal to another node.

Suppose $\sigma_i > \tau_i$ for all $i \in \mathcal{I}$, meaning that we allocate more jamming power than the threshold. Then, we have $\xi_i = \mu_i = 0$ by the complementary slackness condition and (35). Plugging in $\mu_i = \nu_i = 0$ on (34) results in $\lambda_i = 0$, which contradicts (33). Therefore, the optimal point should have $\sigma_i = \tau_i$.

Constraint (31c) now can be viewed as $\rho_i \leq P - \tau_i$. If we assume $\rho_i < P - \tau_i$ for $i \in \mathcal{I}$, then $\mu_i = 0$ to satisfy the complementary slackness condition. Again, we obtain $\lambda_i = 0$ to meet the optimality condition (34), which contradicts to (33).

Combining the above conditions, the optimal transmission and jamming power, ρ_i^* and σ_i^*, are given as

$$\rho_i^* = P - \tau_i, \ \sigma_i^* = \tau_i, \ \forall i \in \mathcal{I}, \tag{36}$$

for τ_i in (30) We correspondingly denote the optimal spectral efficiency as $\gamma^*_{(i,j)}$ by putting ρ_i^* into (11).

The following theorem guarantees that the RRM in (27) and (36) is optimal for the given graph $\mathcal{G}$:

Theorem 1 (**Global optimality of RRM).** *Let $\mathcal{G}$ be a fixed network topology. Then, the solution $(\beta^*_{(i,j),u}, \rho_i^*, \sigma_i^*)$ obtained by solving $\mathcal{P}\mathbf{1}$ under the given $\mathcal{G}$ is globally optimal.*

Proof. The objective function $1/\eta$ in $\mathcal{P}\mathbf{2}$ is convex for $\eta > 0$, and the constraints (23b) and (23c) are affine. Thus, the KKT conditions serve as both necessary and sufficient conditions, guaranteeing $\beta^*_{(i,j),u}$ is a global optimum solution of $\mathcal{P}\mathbf{2}$. Similarly, in $\mathcal{P}\mathbf{3}$, the objective function is convex, and all constraints including (31c) are affine. Thus, KKT conditions are necessary and sufficient, and the solution (ρ_i^*, σ_i^*) is globally optimal for $\mathcal{P}\mathbf{3}$.

Then, from (27), $\beta^*_{(i,j),u}$ can be expressed as an explicit function of (ρ_i^*, σ_i^*). Therefore, combining these yields the full set of decision variables for $\mathcal{P}\mathbf{1}$ under fixed $\mathcal{G}$ in the max-min throughput problem [48], [49]. □

D. Monte-Carlo Relay Routing

a) Problem formulation: We analytically find the optimal frequency resource $\beta^*_{(i,j),u}$, transmission power ρ_i^*, and jamming power σ_i^* for given graph $\mathcal{E}$. Then, the problem can be reformulated as

$$\max_{\mathcal{G}} \min_{\substack{u\in\mathcal{U}, \\ (i,j)\in\mathcal{E}_u}} B \Big(\sum_{j\in\mathcal{N}} \sum_{u\in\mathcal{U}} \frac{x_{(i,j),u} h_u}{\gamma^*_{(i,j)}} \Big)^{-1} \text{s.t. (14b), (14c).} \tag{37}$$

We convert the SPSC constraint (14b) into an explicit link-distance constraint in the routing graph. This transformation is necessary because SPSC probability does not directly indicate how the graph topology is constrained. Specifically, the SPSC constraint determines the maximum link distance, defined as:

$$D_i = -\frac{\ln \tau_i}{\kappa_i} \left(\frac{P - P_i + n_0}{n_0} \right)^{\frac{2}{\alpha_i}}, \tag{38}$$

where D_i indicates the farthest allowable distance from node i at the maximum jamming power $P - P_i$. Thus, enforcing

$$d^{\mathsf{s}}_{(i,j)} \leq D_i, \quad \forall j \in \mathcal{N} \tag{39}$$

ensures that each link satisfies the required SPSC probability.

Solving the optimization problem in (37) is challenging, as the objective cannot be computed before the graph is completed. As depicted in Fig. 2, determining $\beta^*_{(i,j),u}$, ρ_i^*, and σ_i^*

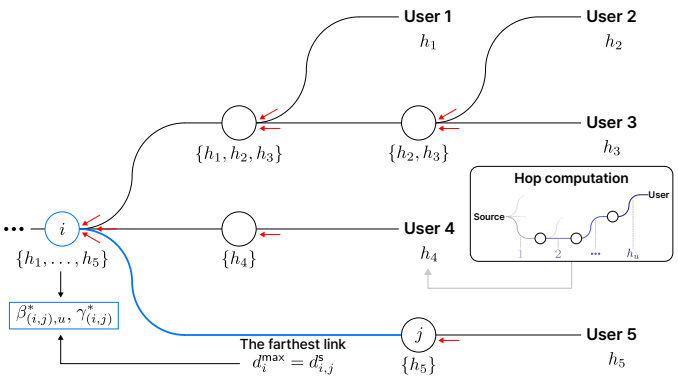

Fig. 2. Visualization of variable flows for node i to optimize radio resources.

requires information, h_u and $x_{(i,j),u}$, from downstream nodes. These variables can be computed only after the complete routing graph $\mathcal{G}$ is established. This interdependence between routing and resource allocation significantly complicates the routing problem.

b) Routing algorithm: This challenge motivates the MCRR in Alg. 1, which builds the relay graph $\mathcal{G}$ by sequentially adding complete source-to-user paths. When a user's path is appended, the user information is upstreamed along the intermediate nodes on the newly added path, as illustrated in Fig. 2. Since the optimal values of $\beta^*_{(i,j),u}$, ρ^*_i, and σ^*_i for the other nodes remain unchanged, their re-optimization can be bypassed. Thus, this design enables the optimization to be node-specific and computationally efficient.

The MCRR in Alg. 1 operates as follows: We first build the initial directed graph $\mathcal{G}_{\text{all}}$ by including all possible edge whose length does not exceed the maximum feasible link distance D_i in Eq. (39) (**Line 1-2**). Then, for each user u, we generate a set of K candidate source-to-user path by collecting a shortest-path on $\mathcal{G}_{\text{all}}$, assigning independent random weights $\mathcal{U}(0,1)$ to edge costs at each iteration (**Line 3-8**). This mechanism thus operates similar to a biased random walk from node 0 toward user u, constructing paths with an proper hop count while exploring topologies that may offer superior performance.

The MCRR refinement process (**Line 9-20**) creates multiple candidate graphs by removing and replacing paths to select the optimal configuration. It begins by temporarily removing the existing path of the user evaluated from the current routing graph (**Line 11-12**). Then, each pre-computed candidate path is inserted once at a time, creating different graph configurations that satisfies ST topology (14c) (**Line 14**). As each change is implemented, its effects immediately propagate through the bandwidth and power allocation equations to upstream nodes (**Line 15**). The algorithm evaluates the minimum throughput of each candidate graph, committing the changes only if the throughput improves; otherwise, it reverts to the original path (**Line 17-18**).

c) Computational complexity of MCRR: Let N be the number of nodes, K the number of candidate paths per user, and R the number of refinement rounds. The computational cost of MCRR is decomposed as follows:

- **Path sampling**: K randomized shortest paths takes the complexity of $\mathcal{O}(KN\log N)$.

Algorithm 1 Monte-Carlo Relay Routing (MCRR)

Require: Nodes $\mathcal{N}$
Ensure: Solution graph $\mathcal{G}^* = (\mathcal{N}^*, \mathcal{E}^*)$
1: $\mathcal{E} \leftarrow \{(i,j) | d^s_{(i,j)} \leq D_i, \forall i,j \in \mathcal{N}\}$, $\mathcal{N}^* \leftarrow \{\}$, $\mathcal{E}^* \leftarrow \{\}$
2: $\mathcal{G}_{\text{all}} \leftarrow (\mathcal{N}, \mathcal{E})$, $\mathcal{G}^* \leftarrow (\mathcal{N}^*, \mathcal{E}^*)$, $T_{\mathcal{G}^*} \leftarrow 0$
3: **for** user u in $\mathcal{U}$ **do**
4: **for** k in $1, \ldots, K$ **do**
5: $\mathcal{E}_{u,k} \leftarrow$ Biased random walk from node 0 to u in $\mathcal{G}_{\text{all}}$
6: $\mathcal{N}_{u,k} \leftarrow$ nodes in the path $\mathcal{P}_{u,k}$
7: **end for**
8: **end for**
9: **while** $T - T_{\mathcal{G}^*} < \epsilon$ **do**
10: **for** each user u **do**
11: $\mathcal{E}_{-u} \leftarrow \{(i,j) \in \mathcal{E}^* | \sum_{u \in \mathcal{U}} x_{(i,j),u} > 1\}$
12: $\mathcal{N}_{-u} \leftarrow \{(i,j) \mid (i,j) \in \mathcal{E}_{-u}\}$
13: **for** k in $1, .., K$ **do**
14: $\mathcal{G}_{u,k} \leftarrow (\mathcal{N}_{-u} \cup \mathcal{N}_{u,k},\ \mathcal{E}_{-u} \cup \mathcal{E}_{u,k})$
15: $T_{\mathcal{G}_{u,k}} \leftarrow \min_{i \in \mathcal{N}_{u,k}} B\Big(\sum_{j \in \mathcal{N}} \sum_{u \in \mathcal{U}} \frac{x_{(i,j),u} h_u}{\gamma^*_{(i,j)}}\Big)^{-1}$
16: **end for**
17: $\mathcal{G}^* \leftarrow \text{argmin}_{\mathcal{G} \in \{\mathcal{G}^*, \mathcal{G}_{u,1}, \ldots, \mathcal{G}_{u,k}\}} T_{\mathcal{G}}$, $(\mathcal{N}^*, \mathcal{E}^*) \leftarrow \mathcal{G}^*$
18: $T \leftarrow \min_{\mathcal{G} \in \{\mathcal{G}^*, \mathcal{G}_{u,1}, \ldots, \mathcal{G}_{u,k}\}} T_{\mathcal{G}}$
19: **end for**
20: **end while**

- **Iterative refinement**: In each of the R rounds, every user examines K candidate paths. For each, the algorithm updates the graph and recomputes throughput by locally propagating changes to relevant upstream nodes. Each operation is lightweight and localized, giving total refinement cost $\mathcal{O}(RNK)$.

Then, total complexity of Alg. 1 is $\mathcal{O}(KN(\log N + R)) \approx \mathcal{O}(KN\log N)$ when $N \gg R$.

V. Numerical Experiments

This section addresses the following research questions:
RQ 1. How accurate is the closed-form approximation of the SPSC probability? ➜ Sec. V-A
RQ 2. How does the max–min throughput in SAGSIN change when security parameters change? ➜ Sec. V-B
RQ 3. How does the proposed framework perform in real-world network deployments? ➜ Sec. V-C

Answering the questions, we broadly provide a comprehensive validation from the feasibility of the system model to the effectiveness of the proposed scheme. Numerical experiments and analysis exploring each question are presented in Sec. V-A to Sec V-C. All simulations are implemented in Python 3.12 on an AMD Ryzen™ 9 5800X processor.

A. Analysis on SPSC Probability Approximation

1) Calibration of the SPSC approximation over Eve density: Fig. 3 shows comparisions of the 50,000 Monte–Carlo evaluations of (5) and its closed–form approximation in (22) for four representative link lengths of $\{50, 100, 200, 400\}$ km.

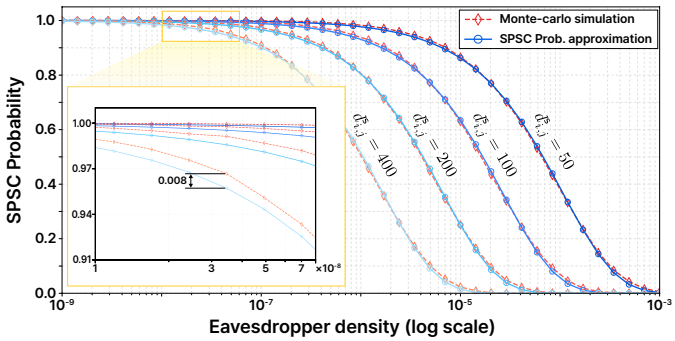

Fig. 3. The SPSC probability versus Eve density for various link distances.

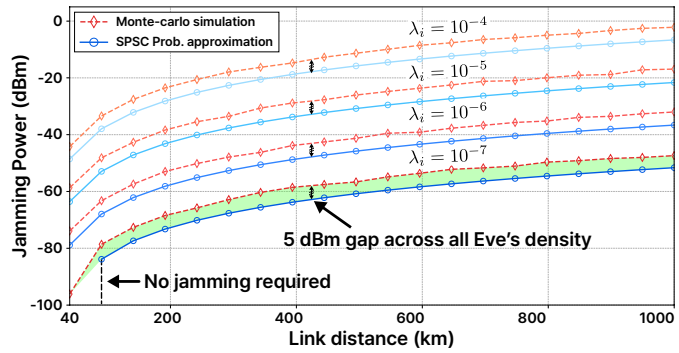

Fig. 5. Required jamming power versus link distance for various Eve densities.

We introduce two distance-dependent parameters a_d and p_d to compensate for the approximation error in the SPSC probability as follows:

$$\mathbb{P}_{(i,j)} = \exp\left[-a_d \kappa_i^{p_d} \left(\frac{n_0}{\sigma_i + n_0}\right)^{\frac{2}{\alpha_i}} \left(d^s_{(i,j)}\right)^2\right]. \tag{40}$$

This correction preserves the correlation between distance and SPSC probability while ensuring accurate estimation under varying Eve densities. The (a_d, p_d) pairs used in our experiments are: $(a_{50}, p_{50}) = (0.224, 0.806)$; $(a_{100}, p_{100}) = (0.170, 0.805)$; $(a_{200}, p_{200}) = (0.133, 0.807)$; and $(a_{400}, p_{400}) = (0.102, 0.807)$.

Across the whole distance range, the analytical expression faithfully tracks the Monte–Carlo result; the largest absolute gap occurring in the inset is < 0.008, confirming that (22) tightly approximates $\mathbb{P}_{(i,j)}$. These results aligns well with the observations from the related work [50].

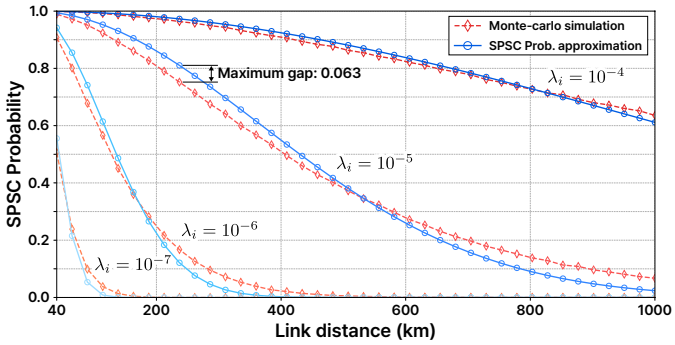

Fig. 4. The SPSC probability versus link distance for various Eve densities.

2) Accuracy of the SPSC approximation over link distance: Fig. 4 benchmarks the SPSC probability obtained from 50,000 Monte–Carlo evaluations of (5) against the closed-form approximation (22) for the four Eve densities $\{10^{-4}, 10^{-5}, 10^{-6}, 10^{-7}\}$ km^{-2}. The largest disparity, 0.063, occurs around 320 km of link distance when $\lambda_i = 10^{-5}$. When the link distance increases, the SPSC approximation shows larger degradation than the Monte-Carlo simulation. This is attributed to the assumption that an infinite number of Eves are distributed over an infinite region, whereas in real environments both the number of Eves and the area are finite.

3) Required jamming power versus link distance: Fig. 5 plots the minimum jamming power to guarantee the target SPSC probability threshold $\tau = 0.9999$. The results are obtained (i) numerically from 500,000 Monte-Carlo simulation of (5) and (ii) via the closed-form inversion (30) of the SPSC approximation.[4]

As shown in Fig. 5, the minimum required jamming power computed by the approximation consistently demonstrates a deviation of approximately 5 dBm across all regions. This trend aligns with the over-estimation of the SPSC approximation in Fig. 4 when the link distance is relatively short. Figs. 3 and 5 collectively suggest that the SPSC approximation (22) needs to be corrected by the computed offset when determining the minimum jamming power in (30) and the maximum link distance in (39).

B. Analysis on Max-Min Throughput

We evaluate the max-min throughput by changing the security parameters and compare the proposed scheme with several baselines. The SAGSIN networks are randomly generated using real-world terrain data across diverse latitudes and longitudes.

a) Baselines: Each baseline employs a different graph-optimization strategy, but they all adopt the same radio resource $\mathbf{B}$, $\mathbf{P}$, and $\mathbf{J}$ as the optimal radio-resource allocation is obtained in Sec. IV.

- **Bruteforce (Naive upper bound):** Exhaustively evaluates all routing graphs to find an upper-bound on minimum throughput. The number of exhaustive search trials is set to 5,000.
- **Hierarchical genetic:** Is a canonical genetic algorithm with elitism [51], but operating in two hierarchical stpdf [52], [53]. In the first step, each node is binary-encoded as a gene to determine the set $\mathcal{N}^*$. The second step determines the set of edges $\mathcal{E}$ by constructing feasible spanning trees among the selected node genes, subject to the graph topology constraints (14c) and the maximum link distance constraint (39). The genetic algorithm is configured as 5,000 generations, 50 populations, 6 elite counts, and 5% mutation probability.

[4]The minimum jamming power is determined using the bisection method. Due to the high variance of the experiments, the number of simulations is increased tenfold.

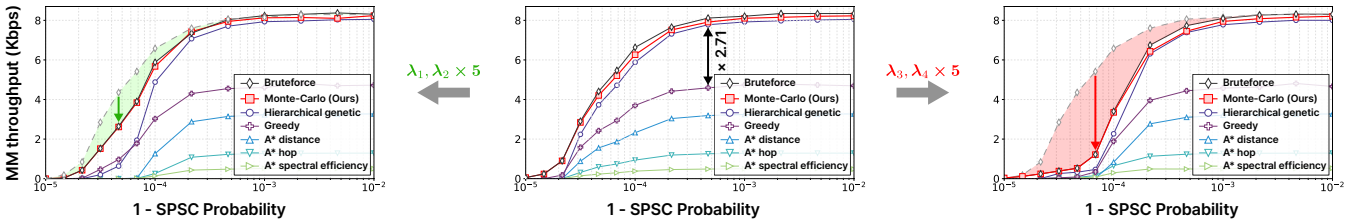

(a) $(\lambda_1, \lambda_2, \lambda_3, \lambda_4) = (5 \cdot 10^{-3}, 10^{-2}, 3 \cdot 10^{-4}, 10^{-4})$ (b) $(\lambda_1, \lambda_2, \lambda_3, \lambda_4) = (10^{-3}, 2 \cdot 10^{-2}, 3 \cdot 10^{-4}, 10^{-4})$ (c) $(\lambda_1, \lambda_2, \lambda_3, \lambda_4) = (10^{-3}, 2 \cdot 10^{-2}, 1.5 \cdot 10^{-3}, 5 \cdot 10^{-4})$

Fig. 6. Max-min throughput versus SPSC outage probability. The grey dashed lines in (a) and (c) represent the numerical results from the brute-force method in (b), illustrating the relative throughput degradation as **green** and **red** areas in (a) and (b) as the Eve density increases. (a) The max-min throughput of the **Bruteforce** scheme at $1-\tau = 5{\cdot}10^{-5}$ decreases from 4.4 kbps in (b) to 2.6 kbps. (c) The performance drop is even more pronounced, with the **Bruteforce** throughput at $1-\tau = 7{\cdot}10^{-5}$ falling from 5.5 kbps to 1.2 kbps.

- **Greedy:** Iteratively selects the relay path that maximizes immediate throughput gain of the user.
- **Variants of A*:** Use fixed link cost metrics in A* search. While these metrics do not exactly optimize $\mathcal{P}\mathbf{1}$ (because the throughput of nodes and edges changes depending on the graph topology), they serve as useful benchmarks for comparing the performance of different schemes. Moreover, graphs generated by A* always have spanning-tree structures [54], ensuring that the graph solutions remain within the feasible domain of $\mathcal{P}\mathbf{1}$.

  The choice of metrics in A* is motivated by the objective function in $\mathcal{P}\mathbf{1}$, which is

  - **A* distance:** Minimizes the summation of the link distances.

  - **A* hop:** Minimizes the number of source-to-user hops.

  - **A* spectral efficiency:** Maximizes the sum spectral efficiency of the source-to-user routes.

TABLE II
SIMULATION PARAMETERS

Parameter (Unit)	Ground (G), Maritime (M), HAPs (H)	LEO
Carrier frequency (GHz)	14	20
Total bandwidth (MHz)	250	400
Tx power (dBm)	30	21.5
Tx antenna gain (dBi)	43.2 (G,M,H→To LEO) 25 (G,M,H→G,M,H)	38.5
Rx antenna gain (dBi)	39.7 (G,M,H→To LEO) 25 (G,M,H→G,M,H)	38.5
Antenna gain to noise temperature (dB/K)	1.5 (H→LEO), 16.2 (H→G,M,H) 1.2 (G,M→LEO), 15.9 (G,M→G,M,H)	13
Pathloss exponent	2.8 (G), 2.7 (M), 2.6 (H)	2.4

b) SAGSIN configurations: The SAGSIN map is generated considering realistic geography as illustrated in Sec. V-C, randomly placing 150 ground base stations, 150 maritime base stations, 12 HAPs stations, and 10 LEO satellites within longitude 30° and latitude 20° to serve 60 users. The default Eve density is set as $(\lambda_1, \lambda_2, \lambda_3, \lambda_4) = (10^{-3}, 2{\cdot}10^{-3}, 3{\cdot}10^{-4}, 10^{-4})$ following the literature [55]. Physical layer parameters for SAGSIN, such as carrier frequency, total bandwidth, antenna gain, and antenna gain-to-noise-temperature, are configured as in Table II, referring to [56], [57] and the 3GPP standard [11].

1) Impact of the SPSC probability threshold: Fig. 6 illustrates how the max-min throughput varies as the SPSC outage probability $(1-\tau)$ increases from 10^{-5} to 10^{-2}. The minimum transmit power P_i for each base station is set to 80% of its total available power. Figs. 6a and 6c are obtained by scaling the Eve densities of ground/maritime nodes; and HAPs/LEO nodes fivefold, relative to Fig. 6b.

The minimum throughput of all schemes converges to zero as $1-\tau$ approaches zero. This is because a tighter SPSC threshold τ reduces the maximum link distance (39), making some users unserviceable. Across all subfigures, the proposed **Monte-Carlo** scheme consistently attains throughput levels within ≈5% of the optimal values achieved by the **Bruteforce** method, demonstrating both its efficiency and near-optimal performance.

In Figs. 6a and 6c, we note that the increase in the Eve density of HAPs and LEO notably deteriorate the max-min throughput, inducing a long tail near zero throughput. This result verifies the critical role of HAPs and LEO nodes in forming secure relays in SAGSINs, as they can establish long-distance connections more easily due to their low path loss and line-of-sight characteristics.

2) Impact of Eve density: Fig. 7 shows how the max-min throughput changes when Eve densities in the various SAGSIN layers vary. The SPSC probability threshold τ is fixed at 99.99%. In all subfigures, the max-min throughput improves as the Eve density decreases. This improvement is attributed to the expansion of the feasible region defined by the constraints in $\mathcal{P}\mathbf{1}$, thereby providing a broader set of relay options to achieve higher user throughput.

Nevertheless, as shown in Figs. 7a, b, and e, the max-min throughputs of ground and maritime nodes exhibit only modest throughput improvement relative to those of HAPS and LEO nodes. Although the large number of ground and maritime nodes expands the search space and theoretically offers more routing possibilities, it also significantly increases algorithmic complexity and reduces the likelihood of reaching the global optimum. Consequently, the additional computational burden offsets the expected throughput gain due to increased search complexity, leading to only modest improvements. In Figs. 7d, f, and g, the most significant throughput increases are observed when reducing the Eve density at the LEO layer, as LEO nodes enable source-to-user connections with fewer hops and higher spectral efficiency through inter-satellite routes.

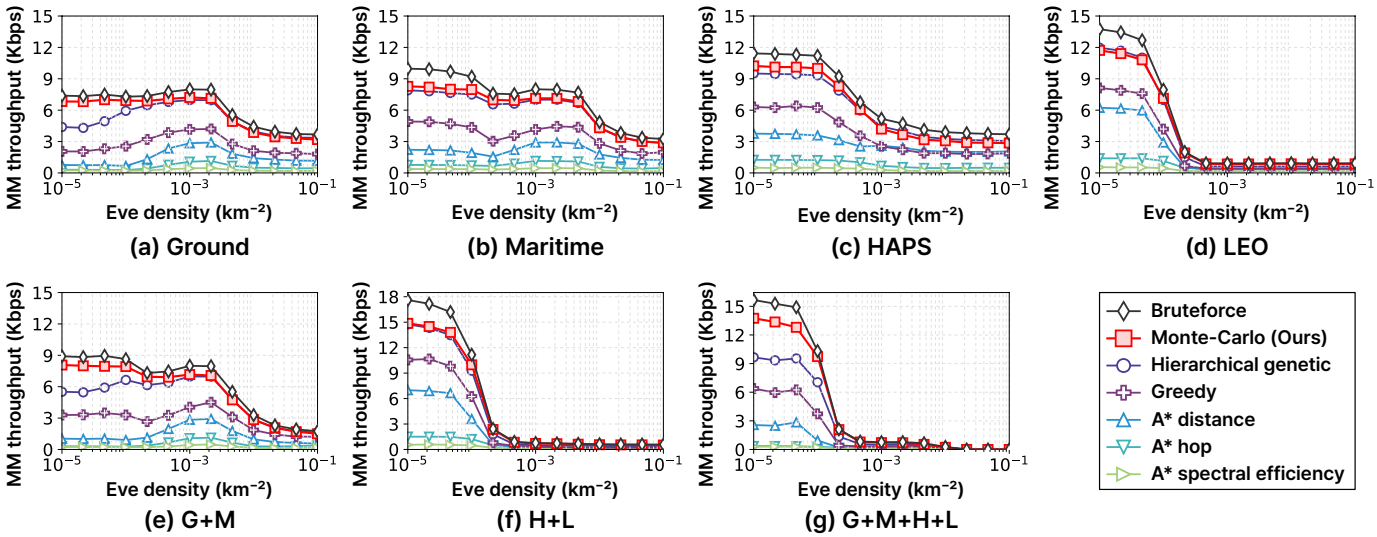

Fig. 7. Max-min throughput versus Eve density for various SAGSIN scenario. Each graph reports the max–min throughput while varying the Eve density of the infrastructure layer indicated in the caption, with the other layers fixed at $(\lambda_1, \lambda_2, \lambda_3, \lambda_4) = (10^{-3}, 2{\cdot}10^{-3}, 3{\cdot}10^{-4}, 10^{-4})$. Notations **G+M**, **H+L**, and **G+M+H+L** in (e), (f), and (g) correspond to ground and maritime; haps and leo;, and ground, maritime, haps and leo, respectively.

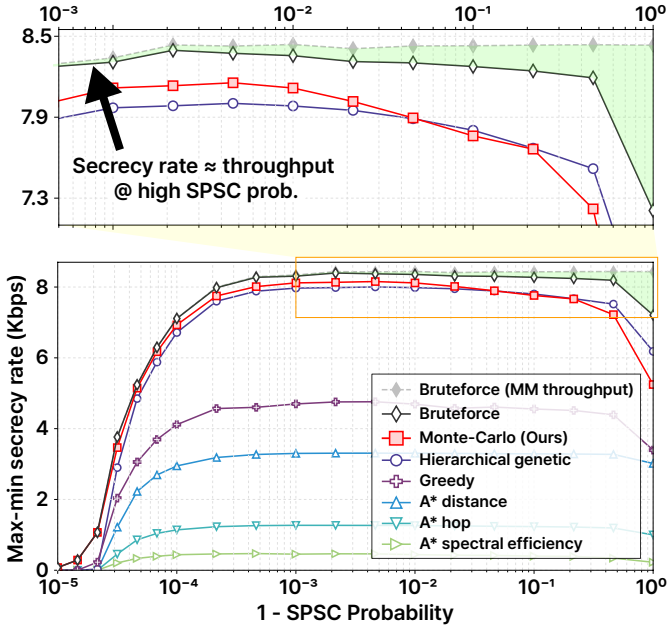

Fig. 8. Comparison of max-min throughput and secrecy rate versus SPSC outage probability. The lower graph plots the max-min secrecy rates across the SPSC probabilities, while the upper graph magnifies the gap (**Green area**) between the max-min throughput and secrecy rate for the brute-force solution.

3) Throughput-secrecy gap: Fig. 8 presents a comparative analysis between the max-min secrecy rate and the max-min throughput across varying SPSC probability thresholds. As the threshold τ increases, the two metrics exhibit a strong convergence, which highlights their equivalence under stringent security constraints. In contrast, in the regime of low SPSC thresholds, a noticeable performance gap occurs, primarily because the max-min throughput formulation does not intrinsically incorporate relay security considerations. However, maintaining a high SPSC probability (e.g., > 0.95) is imperative to effectively mitigate the risk of eavesdropping by adversarial nodes such as Eve [44]. Under the high-security regime, where the SPSC probability exceeds a predefined reliability threshold, the maximum throughput-secrecy gap is approximately 0.38% at $1 - \tau = 10^{-3}$, which is marginal enough to justify the use of max-min throughput metric in highly secure scenarios.

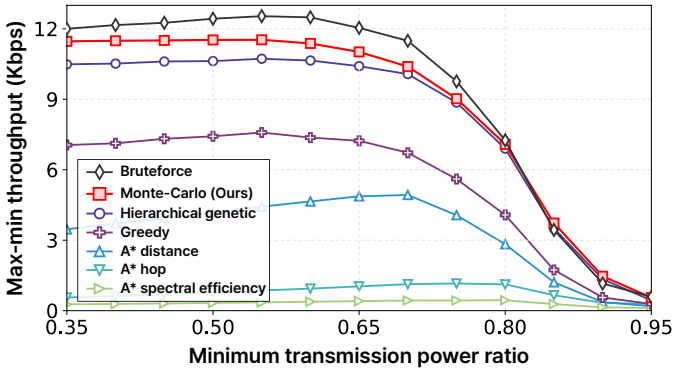

Fig. 9. Max–min throughput versus minimum transmit power ratio.

4) Impact of minimum transmit-power constraint: Fig. 9 examines how the max–min throughput varies as the minimum transmission power ratio P_i/P changes. For $P_i/P < 0.65$, each node can flexibly allocate its transmission and jamming powers according to (36), thereby maintaining a nearly constant achievable throughput.

This finding suggests a practical design guideline as follows: As P_i increases, the maximum available jamming budget gradually decreases, which shortens the admissible link distance under the SPSC constraint and excessively limits the feasible graph domain. Selecting P_i/P within the range of 0.6-0.7 ensures adequate jamming capability while eliminating non-promising links, thereby reducing the search space without compromising performance.

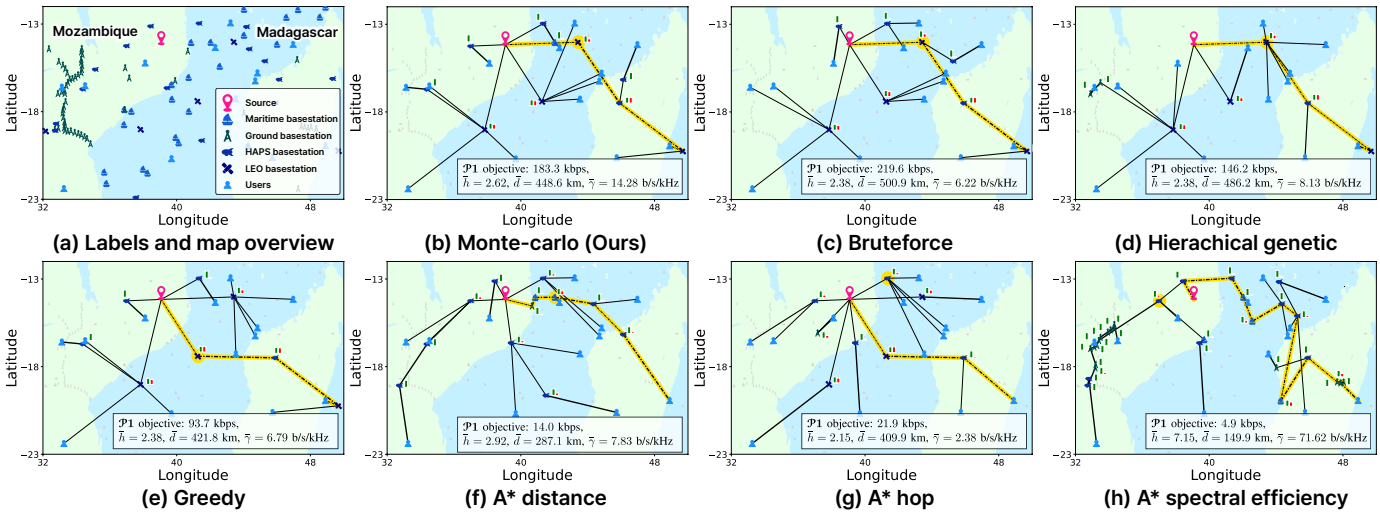

Fig. 10. Secure routing examples on the Mozambique-Madagascar testbed. The highlighted dashed line represents the longest path. The highlighted node represents the min-throughput node. $\bar{h}$, $\bar{d}$, and $\bar{\gamma}$ represent average hop, link distance, and link spectral efficiency, respectively. The green and red bars adjacent to each node indicate the normalized transmission and jamming power allocated under the minimum transmission power ratio $P_i/P = 0.8$. The line width of each link represents the amount of allocated bandwidth.

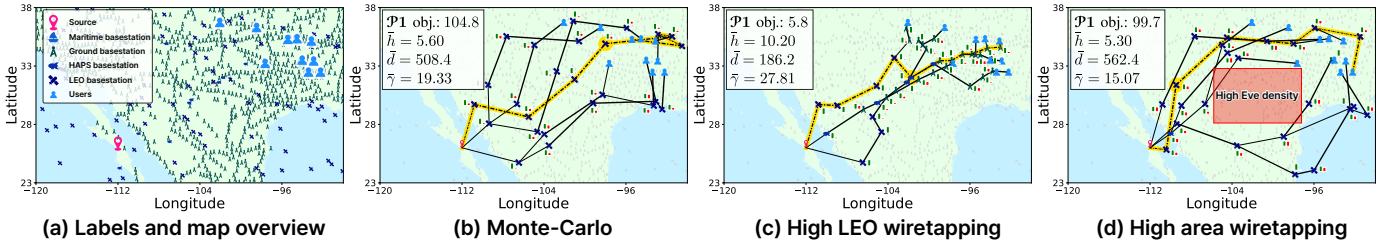

Fig. 11. Secure routing solutions on the Southern North America testbed. (a) Moderate uniform Eve density; (b) High Eve density in the LEO layer; (c) Localized high-density region (**red area**). Eve density in (b) and (c) is increased tenfold. Markers and annotations follow those in Fig. 10.

C. Demonstrations on Real-World Data Testbeds

We evaluate and visualize the framework in testbeds built from real-world data to understand how each scheme operates and how the framework behaves when the secure environment changes. We construct two testbeds in the Mozambique-Madagascar Channel and Southern North America. This work is the first to establish **a real-world SAGSIN testbed** integrating HAP base stations. This is significant as it accurately reflects the large-scale mobility patterns of HAPs [58].[5]

a) Data preparation: The testbeds incorporate various network elements from multiple data sources, as detailed below:

- **Ground.** Ground node positions are extracted from the open source project OPENCELLID database, using a network snapshot at 2025-04-22 13:00 UTC.
- **Maritime.** Maritime nodes for the Mozambique-Madagascar testbed are parsed from the MARINETRAFFIC database at 2025-04-22 13:00 UTC.
- **HAPs.** HAPs node positions are derived from the non-profit organization STRATOCAT database based on data provided by Google's Project Loon [58]. Snapshots at 2020-09-28 10:00 UTC for Mozambique-Madagascar; and at 2020-07-29 00:00 UTC for Southern North America are used to represent HAPs deployments.
- **LEO satellites.** LEO node coordinates are extracted from the non-profit organization CELESTRAK repository, parsing Starlink satellites at 2025-04-22 13:00 UTC.

All datasets are processed through a unified environment generator that filters, subsamples, and formats the raw inputs into simulation-ready node lists.

1) Mozambique-Madagascar Testbed: Fig. 10 overlays the secure routes selected in the Mozambique–Madagascar testbed. In Fig. 10b, the proposed **Monte-Carlo** scheme consistently finds the "sweet-spot" of two or three hops of a few hundred kilometers each, thereby balancing the throughput penalty of extra relay hops with the signal loss incurred on longer links.

Simple static metrics (**A* distance, hop, or spectral efficiency**) provide useful insights, but optimizing only one axis inevitably violates the inherent multi-dimensional trade-offs. **A* hop** forces overly long links that suffer severe SNR penalties, while **A* spectral efficiency** fragments the path into many short hops and incur excessive scheduling overhead. These observations reveal that effective secure routing in SAGSIN must jointly account for hop count, link distance, and per-hop capacity.

[5]Since no operational datasets for HAP base stations are currently available, the HAPs nodes were synthesized with temporal adjustments.

2) Southern North America testbed: Fig. 11 shows how the proposed MCRR adapts to varying Eve distributions in the Southern North America region. By computing each link's maximum allowable distance from Eve density and the SPSC threshold, the framework automatically adjusts routing when (i) density increases on a particular network layer (Fig. 11c) and (ii) Eves concentrate in a specific geographic area (Fig. 11d). Thus, we can observe:

- **Fig. 11b:** When Eve density is moderate across all layers, the **Monte-Carlo** scheme adopts inter-satellite paths that maintain throughput in the hundreds of kbps.
- **Fig. 11c:** If Eve density spikes around LEO satellites, those links become infeasible under the distance constraint, and the algorithm detours via ground and HAPs nodes.
- **Fig. 11d:** When Eves concentrate in the shaded area, links crossing that region are automatically excluded and replaced by detours around the area.

In summary, incorporating distance constraints computed from the Eve density and the SPSC threshold into the optimization process enables routing decisions to promptly adapt to variations in node-specific and geographical secure threats.

VI. Conclusion

This work demonstrates that secure and high-performance multi-hop communication can be achieved even in the presence of unknown eavesdroppers across large-scale SAGSINs. This achievement is made possible by deriving a closed-form expression for the SPSC probability and integrating it into a cross-layer optimization framework that jointly optimizes radio resources and relay routes. This framework features an $\mathcal{O}(1)$-complexity frequency allocation and power splitting strategy, along with a Monte Carlo relay routing algorithm that ensures a minimum throughput for each user under security constraints. The proposed framework was validated through a real-world testbed incorporating ground, maritime, HAP, and LEO nodes, marking the first SAGSIN testbed that includes HAP base stations. This validation narrows the gap between theoretical models and practical deployment, offering promising insights into the realization of secure communication in future 6G integrated networks. Building on these results, future research directions include the development of adaptive secure routing schemes under dynamic network variations, the enhanced integration of heterogeneous network layers, and the transition toward practical system implementations.

Appendix A
Derivation of the SPSC Probability

Lemma 1. $\int_{\mathbb{R}^2} \frac{c}{\|\boldsymbol{x}\|_2^\alpha + c} d\boldsymbol{x} = \sin^{-1}\left(\frac{2}{\alpha}\pi\right) \cdot c^{2/a}$ *for some constant* c.

Proof. Converting the Cartesian coordinate into shpreical coordinate results in

$$\begin{aligned}
\int_{\mathbb{R}^2} \frac{c}{\|\boldsymbol{x}\|_2^\alpha + c} d\boldsymbol{x} &= \int_0^\infty \int_0^{2\pi} \frac{cr}{r^\alpha + c}\, d\theta dr \\
&\overset{(a)}{=} 2\pi \int_0^\infty \frac{cr}{r^\alpha + c}\, dr = \frac{2\pi}{\alpha} c^{\frac{2}{\alpha}} \int_0^\infty \frac{s^{\frac{2}{\alpha}-1}}{s+1}\, ds \\
&= \frac{2\pi}{\alpha} c^{\frac{2}{\alpha}} \int_0^\infty \int_0^\infty s^{\frac{2}{\alpha}-1} \exp(-(s+1)t)\, dsdt \\
&= \frac{2\pi}{\alpha} c^{\frac{2}{\alpha}} \int_0^\infty \exp(-t) \int_0^\infty s^{\frac{2}{\alpha}-1} \exp(-st)\, dsdt \\
&= \frac{2\pi}{\alpha} c^{\frac{2}{\alpha}} \int_0^\infty t^{-\frac{2}{\alpha}} \exp(-t) \Gamma(\frac{2}{\alpha})\, dt \\
&= \frac{2\pi}{\alpha} c^{\frac{2}{\alpha}} \Gamma(1 - \frac{2}{\alpha}) \Gamma(\frac{2}{\alpha}) \\
&= \pi \sin^{-1}(\frac{2}{\alpha}\pi) \cdot c^{\frac{2}{\alpha}}.
\end{aligned} \tag{41}$$

Equation (a) holds by substituting $s = r^\alpha / c$ into the expression. As a result, plugging in $\alpha = \alpha_i$ and $c = \frac{n_0}{\sigma_i + n_0} (d^{\mathsf{s}}_{(i,j)})^{\alpha_i}$ leads to (22). □

References

[1] O. Kodheli, E. Lagunas, N. Maturo, S. K. Sharma, B. Shankar, J. F. M. Montoya, J. C. M. Duncan, D. Spano, S. Chatzinotas, S. Kisseleff, J. Querol, L. Lei, T. X. Vu, and G. Goussetis, "Satellite communications in the new space era: A survey and future challenges," *IEEE Commun. Surveys Tuts.*, vol. 23, no. 1, pp. 70–109, 2021.

[2] M. G. Bellemare, S. Candido, P. S. Castro, J. Gong, M. C. Machado, S. Moitra, S. S. Ponda, and Z. Wang, "Autonomous navigation of stratospheric balloons using reinforcement learning," *Nature*, vol. 588, no. 7836, pp. 77–82, December 2020. [Online]. Available: https://doi.org/10.1038/s41586-020-2939-8

[3] M. Elamassie and M. Uysal, "FSO-based multi-layer airborne backhaul networks," *IEEE Trans. Veh. Technol.*, vol. 73, no. 10, pp. 15 004–15 019, 2024.

[4] Y. Li, J. Xu, N. Khachatrian, and M.-S. Alouini, "Implementation of an ieee 802.11ax-based maritime mesh network in the red sea," 2025. [Online]. Available: https://arxiv.org/abs/2502.13559

[5] J. Zhang, S. Wang, Z. Ma, G. Gao, Y. Guo, F. Zhang, S. Huang, and J. Zhang, "Long-term and real-time high-speed underwater wireless optical communications in deep sea," *IEEE Commun. Mag.*, vol. 62, no. 3, pp. 96–101, 2024.

[6] S. Meng, S. Wu, J. Zhang, J. Cheng, H. Zhou, and Q. Zhang, "Semantics-empowered space-air-ground-sea integrated network: New paradigm, frameworks, and challenges," *IEEE Commun. Surveys Tuts.*, vol. 27, no. 1, pp. 140–183, 2025.

[7] H. Guo, J. Li, J. Liu, N. Tian, and N. Kato, "A survey on space-air-ground-sea integrated network security in 6G," *IEEE Commun. Surveys Tuts.*, vol. 24, no. 1, pp. 53–87, 2022.

[8] ITU-R WP5D, "M.2160: framework and overall objectives of the future development of IMT for 2030 and beyond," ITU Radiocommunication Sector (ITU-R), ITU-R recommendations, Nov. 2023. [Online]. Available: https://www.itu.int/rec/R-REC-M.2160/en

[9] 3rd Generation Partnership Project (3GPP), "Study on 5GC Enhancements for Non-Terrestrial Networks (NTN)," 3GPP, Technical Report 3GPP TR 23.700-10, October 2023. [Online]. Available: https://www.3gpp.org/ftp/Specs/archive/23_series/23.700-10/

[10] ——, "5G Media Streaming – Support for Non-Terrestrial Networks (NTN)," 3GPP, Technical Specification 3GPP TS 26.501, January 2024. [Online]. Available: https://www.3gpp.org/ftp/Specs/archive/26_series/26.501/

[11] ——, "Solutions for NR to support Non-Terrestrial Networks (NTN) - Enhancements in Release 18," 3GPP, Technical Report 3GPP TR 38.821, February 2024. [Online]. Available: https://www.3gpp.org/ftp/Specs/archive/38_series/38.821/

[12] Q. Wang, H. Wang, W. Sun, N. Zhao, H.-N. Dai, and W. Zhang, "Aerial bridge: A secure tunnel against eavesdropping in terrestrial-satellite networks," *IEEE Trans. Wireless Commun.*, vol. 22, no. 11, pp. 8096–8113, 2023.

[13] C. Han, L. Bai, T. Bai, and J. Choi, "Joint UAV deployment and power allocation for secure space-air-ground communications," *IEEE Trans. Commun.*, vol. 70, no. 10, pp. 6804–6818, 2022.

[14] Y. Zhang, X. Gao, H. Yuan, K. Yang, J. Kang, P. Wang, and D. Niyato, "Joint UAV trajectory and power allocation with hybrid FSO/RF for secure space–air–ground communications," *IEEE Internet Things J.*, vol. 11, no. 19, pp. 31 407–31 421, 2024.

[15] H. Li, J. Li, M. Liu, and F. Gong, "UAV-assisted secure communication for coordinated satellite-terrestrial networks," *IEEE Commun. Lett.*, vol. 27, no. 7, pp. 1709–1713, 2023.

[16] Z. Wang, Z. Yin, X. Wang, N. Cheng, Y. Zhang, and T. H. Luan, "Label-free deep learning driven secure access selection in space-air-ground integrated networks," in *IEEE Global Commun. Conf. (GLOBECOM)*, 2023, pp. 958–963.

[17] A. Kakati, G. Li, E. Moustapha Diallo, L. Chiru Kawala, N. Hussain, and A. B. M. Adam, "Toward proactive, secure and efficient space-air-ground communications: Generative AI-based DRL framework," *IEEE Open J. Commun. Soc.*, vol. 6, pp. 1284–1298, 2025.

[18] G. Sun, J. Li, A. Wang, Q. Wu, Z. Sun, and Y. Liu, "Secure and energy-efficient UAV relay communications exploiting collaborative beamforming," *IEEE Trans. Commun.*, vol. 70, no. 8, pp. 5401–5416, 2022.

[19] T. N. Nguyen, T. Van Chien, D.-H. Tran, V.-D. Phan, M. Voznak, S. Chatzinotas, Z. Ding, and H. V. Poor, "Security-reliability tradeoffs for satellite–terrestrial relay networks with a friendly jammer and imperfect CSI," *IEEE Trans. Aerosp. Electron. Syst.*, vol. 59, no. 5, pp. 7004–7019, 2023.

[20] H.-N. Dai, Y. Wu, M. Imran, and N. Nasser, "Integration of blockchain and network softwarization for space-air-ground-sea integrated networks," *IEEE Internet Things Mag.*, vol. 5, no. 1, pp. 166–172, 2022.

[21] P. Xu, G. Chen, J. Quan, C. Huang, I. Krikidis, K.-K. Wong, and C.-B. Chae, "Deep learning driven buffer-aided cooperative networks for B5G/6G: Challenges, solutions, and future opportunities," *IEEE Wireless Commun.*, vol. 31, no. 4, pp. 215–222, 2024.

[22] L. Dong, Z. Han, A. P. Petropulu, and H. V. Poor, "Improving wireless physical layer security via cooperating relays," *IEEE Trans. Signal Processing*, vol. 58, no. 3, pp. 1875–1888, 2010.

[23] Y. Su, L. Li, R. Fan, Y. Liu, and Z. Jin, "A secure transmission scheme with energy-efficient cooperative jamming for underwater acoustic sensor networks," *IEEE Sensors J.*, vol. 22, no. 21, pp. 21 287–21 298, 2022.

[24] A. S. Abdalla, A. Behfarnia, and V. Marojevic, "UAV trajectory and multi-user beamforming optimization for clustered users against passive eavesdropping attacks with unknown CSI," *IEEE Trans. Veh. Technol.*, vol. 72, no. 11, pp. 14 426–14 442, 2023.

[25] M. H. Eiza and A. Raschellà, "A hybrid SDN-based architecture for secure and QoS aware routing in space-air-ground integrated networks (SAGINs)," in *IEEE Wireless Commun. Networking Conf. (WCNC)*, 2023, pp. 1–6.

[26] H. Luo, Y. Wu, G. Sun, H. Yu, and M. Guizani, "ESCM: An efficient and secure communication mechanism for UAV networks," *IEEE Trans. Netw. Serv. Manag.*, vol. 21, no. 3, pp. 3124–3139, 2024.

[27] M. Sbeiti, N. Goddemeier, D. Behnke, and C. Wietfeld, "PASER: Secure and efficient routing approach for airborne mesh networks," *IEEE Trans. Wireless Commun.*, vol. 15, no. 3, pp. 1950–1964, 2016.

[28] K. Guo, K. An, B. Zhang, Y. Huang, and D. Guo, "Physical layer security for hybrid satellite terrestrial relay networks with joint relay selection and user scheduling," *IEEE Access*, vol. 6, pp. 55 815–55 827, 2018.

[29] T. Cover and A. Gamal, "Capacity theorems for the relay channel," *IEEE Trans. Inform. Theory*, vol. 25, no. 5, pp. 572–584, 1979.

[30] P. Gupta and P. Kumar, "The capacity of wireless networks," *IEEE Trans. Inform. Theory*, vol. 46, no. 2, pp. 388–404, 2000.

[31] S. Goel and R. Negi, "Guaranteeing secrecy using artificial noise," *IEEE Trans. Wireless Commun.*, vol. 7, no. 6, pp. 2180–2189, 2008.

[32] L. Lv, H. Jiang, Z. Ding, L. Yang, and J. Chen, "Secrecy-enhancing design for cooperative downlink and uplink NOMA with an untrusted relay," *IEEE Trans. Commun.*, vol. 68, no. 3, pp. 1698–1715, 2020.

[33] B. Chen, R. Li, Q. Ning, K. Lin, C. Han, and V. C. Leung, "Security at physical layer in NOMA relaying networks with cooperative jamming," *IEEE Trans. Veh. Technol.*, vol. 71, no. 4, pp. 3883–3888, 2022.

[34] Y. Mao, H. Zhao, W. Li, and S. Shao, "Joint transceiver optimization for CJ-aided security communication systems with frequency mismatch," *IEEE Wireless Commun. Lett.*, vol. 13, no. 6, pp. 1631–1635, 2024.

[35] F. Jameel, S. Wyne, G. Kaddoum, and T. Q. Duong, "A comprehensive survey on cooperative relaying and jamming strategies for physical layer security," *IEEE Commun. Surveys Tuts.*, vol. 21, no. 3, pp. 2734–2771, 2019.

[36] L. Kong, S. Vuppala, and G. Kaddoum, "Secrecy analysis of random MIMO wireless networks over α-μ fading channels," *IEEE Trans. Veh. Technol.*, vol. 67, no. 12, pp. 11 654–11 666, 2018.

[37] Y. J. Tolossa, S. Vuppala, G. Kaddoum, and G. Abreu, "On the uplink secrecy capacity analysis in D2D-enabled cellular network," *IEEE Systems J.*, vol. 12, no. 3, pp. 2297–2307, 2018.

[38] N. Bhargav, S. L. Cotton, and D. E. Simmons, "Secrecy capacity analysis over $\kappa - \mu$ fading channels: Theory and applications," *IEEE Trans. Commun.*, vol. 64, no. 7, pp. 3011–3024, 2016.

[39] M. Pagin, T. Zugno, M. Polese, and M. Zorzi, "Resource management for 5G NR integrated access and backhaul: A semi-centralized approach," *IEEE Trans. Wireless Commun.*, vol. 21, no. 2, pp. 753–767, 2022.

[40] H. Yin, S. Roy, and L. Cao, "Routing and resource allocation for IAB multi-hop network in 5G advanced," *IEEE Trans. Commun.*, vol. 70, no. 10, pp. 6704–6717, 2022.

[41] 3rd Generation Partnership Project (3GPP), "NG-RAN; Architecture description," 3rd Generation Partnership Project (3GPP), Tech. Rep. TS 38.401, March 2023. [Online]. Available: https://www.3gpp.org/ftp/Specs/archive/38_series/38.401/

[42] ——, "NR; Integrated Access and Backhaul (IAB) architecture and procedures," 3rd Generation Partnership Project (3GPP), Tech. Rep. TS 38.340, June 2023. [Online]. Available: https://www.3gpp.org/ftp/Specs/archive/38_series/38.340/

[43] J. Yao and Y. Liu, "Secrecy rate maximization with outage constraint in multihop relaying networks," *IEEE Commun. Lett.*, vol. 22, no. 2, pp. 304–307, 2018.

[44] J. Yao, X. Zhou, Y. Liu, and S. Feng, "Secure transmission in linear multihop relaying networks," *IEEE Trans. Wireless Commun.*, vol. 17, no. 2, pp. 822–834, 2018.

[45] S. Thapar, D. Mishra, and R. Saini, "Novel outage-aware NOMA protocol for secrecy fairness maximization among untrusted users," *IEEE Trans. Veh. Technol.*, vol. 69, no. 11, pp. 13 259–13 272, 2020.

[46] Y. Xu, J. Liu, Y. Shen, X. Jiang, and T. Taleb, "Security/QoS-aware route selection in multi-hop wireless ad hoc networks," in *IEEE Int. Conf. on Commun. (ICC)*, 2016, pp. 1–6.

[47] Y. Xu, J. Liu, O. Takahashi, N. Shiratori, and X. Jiang, "SOQR: Secure optimal QoS routing in wireless ad hoc networks," in *IEEE Wireless Commun. Netw. Conf. (WCNC)*, 2017, pp. 1–6.

[48] S. Boyd and L. Vandenberghe, *Convex Optimization*. Cambridge University Press, March 2004.

[49] X. Gong, S. A. Vorobyov, and C. Tellambura, "Joint bandwidth and power allocation with admission control in wireless multi-user networks with and without relaying," *IEEE Trans. Signal Processing*, vol. 59, no. 4, pp. 1801–1813, 2011.

[50] J. Yao, S. Feng, X. Zhou, and Y. Liu, "Secure routing in multihop wireless ad-hoc networks with decode-and-forward relaying," *IEEE Trans. Commun.*, vol. 64, no. 2, pp. 753–764, 2016.

[51] T. Weise, "Global optimization algorithms-theory and application," *Self-Published Thomas Weise*, vol. 361, 2009.

[52] R. Schaefer and J. Kolodziej, "Genetic search reinforced by the population hierarchy," in *Foundations of Genetic Algorithms 7*. San Francisco, CA, USA: Morgan Kaufmann Publishers, 2003, pp. 383–399.

[53] E. Ciepiela, J. Kocot, L. Siwik, and R. Dreżewski, "Hierarchical approach to evolutionary multi-objective optimization," in *Int. Conf. Comput. Sci. (ICCS)*, M. Bubak, G. D. van Albada, J. Dongarra, and P. M. A. Sloot, Eds. Berlin, Heidelberg: Springer Berlin Heidelberg, 2008, pp. 740–749.

[54] T. H. Cormen, C. E. Leiserson, R. L. Rivest, and C. Stein, "Dijkstra's algorithm," in *Introduction to Algorithms*, 3rd ed. MIT Press, 2009, ch. 24.3, pp. 658–664.

[55] Y. Zou, J. Zhu, X. Wang, and L. Hanzo, "A survey on wireless security: Technical challenges, recent advances, and future trends," *Proc. IEEE*, vol. 104, no. 9, pp. 1727–1765, 2016.

[56] D. Liu, J. Zhang, J. Cui, S.-X. Ng, R. G. Maunder, and L. Hanzo, "Deep learning aided routing for space-air-ground integrated networks relying on real satellite, flight, and shipping data," *IEEE Wireless Commun.*, vol. 29, no. 2, pp. 177–184, 2022.

[57] M. Vondra, M. Ozger, D. Schupke, and C. Cavdar, "Integration of satellite and aerial communications for heterogeneous flying vehicles," *IEEE Netw.*, vol. 32, no. 5, pp. 62–69, 2018.

[58] M. G. Bellemare, S. Candido, P. S. Castro, J. Gong, M. C. Machado, S. Moitra, S. S. Ponda, and Z. Wang, "Autonomous navigation of stratospheric balloons using reinforcement learning," *Nature*, vol. 588, pp. 77–82, 2020.